

# Fe-vacancy Ordered Fe<sub>4</sub>Se<sub>5</sub>—The Insulating Parent Phase of FeSe Superconductor

Keng-Yu Yeh<sup>1,2,4</sup>, Yan-Rai Chen<sup>1,2,4</sup>, Tung-Sheng Lo<sup>1</sup>, Phillip M. Wu<sup>1,5</sup>, Ming-Jye Wang<sup>1,3</sup>, Kuei-Shu Chang-Liao<sup>4</sup>, and Maw-Kuen Wu<sup>1\*</sup>

<sup>1</sup>Institute of Physics, Academia Sinica, Taipei 115, Taiwan

<sup>2</sup>Taiwan International Graduate Student Program, Academia Sinica, Taipei 115, Taiwan

<sup>3</sup>Institute of Astronomy and Astrophysics, Academia Sinica, Taipei 115, Taiwan

<sup>4</sup>Department of Engineering and System Science, National Tsing Hua University, Hsinchu 300, Taiwan

<sup>5</sup>BitSmart LLC, San Mateo CA 94403, USA

## \* Correspondence:

Maw-Kuen Wu

mkwu@phys.sinica.edu.tw

**Keywords:** FeSe superconductors, Verwey-like transition, Fe-vacancy order, Mott insulators, Mix-valence state

## Abstract

We have carried out a detailed study to investigate the existence of an insulating parent phase for FeSe superconductor. The insulating Fe<sub>4</sub>Se<sub>5</sub> with  $\sqrt{5} \times \sqrt{5}$  Fe-vacancy order shows a 3D-Mott variable range hopping behavior with a Verwey-like electronic correlation at around 45 K. The application of the RTA process at 450 °C results in the destruction of Fe-vacancy order and induces more electron carriers by increasing the Fe<sup>3+</sup> valence state. Superconductivity emerges with  $T_c \sim 8$ K without changing the chemical stoichiometry of the sample after the RTA process by resulting in the addition of extra carriers in favor of superconductivity.

## 1 Introduction

The FeAs-based [1] and FeSe-based [2] superconductors are among the most investigated materials in condensed matter physics since their discovery in 2008. The observation of a wide range of superconducting transition temperatures, with the highest confirmed Cooper pair formation temperature up to 75 K in monolayer FeSe film [3] provides a unique opportunity to gain more insight into the origin of high-temperature superconductivity. The multiple-orbital nature of the Fe-based materials, combined with spin and charge degrees of freedom, results in the observation of many intriguing phenomena such as structural distortion, magnetic or orbital ordering [4], and electronic nematicity [5, 6]. There are suggestions that the orbital fluctuation may provide a new channel for realizing superconductivity [7, 8].

The parent compounds of FeAs-based materials exhibit structural transitions from a high-temperature tetragonal phase to a low-temperature orthorhombic phase, which accompanies with an antiferromagnetic (AF) order [9, 10]. Upon doping, both the orthorhombic structure and the AF phase

are suppressed and superconductivity is induced. On the other hand, FeSe undergoes a tetragonal-to-orthorhombic transition at  $\sim 90$  K [2, 11, 12]. However, no magnetic order is formed at ambient pressure [12, 13] and superconductivity below  $\sim 8$  K [2] is crucially related to this orthorhombic distortion. The nematic order coexists with superconductivity but not with long-range magnetic order has led to arguments that the origin of the nematicity in FeSe is not magnetically but likely orbital-driven [14, 15].

However, recent studies show that the nematic states in the FeSe systems are far more complex [16–20]. There exist strong high-energy spin fluctuations [20] which suggest that the nematicity and magnetism may be still intimately linked. It was also found that there are many interesting features in the band structures of the nematic state. More surprises came as one applied pressure to FeSe. The application of pressure leads to the suppression of structural transition, the appearance of a magnetically ordered phase at  $\sim 1$  GPa [13, 21], and  $T_c$  increases to a maximum  $\sim 37$  K [22–27] at  $\sim 6$  GPa. An even more dramatic enhancement of  $T_c$  was achieved on monolayer FeSe grown on SrTiO<sub>3</sub> substrate [28–31]

The above observations lead to questions that exist since the discovery of FeSe superconductor: what is the exact chemical stoichiometry of the compound, and what is the exact phase diagram for the FeSe system? Earlier studies showed that the superconducting property of FeSe is very sensitive to its stoichiometry [2, 12, 32]. The fact that higher superconducting transition temperature exists in monolayer FeSe on SrTiO<sub>3</sub> substrate suggests that the commonly accepted phase diagram, derived from assuming that FeTe is the non-superconducting parent compound of FeSe [33], is questionable. Studies have observed the trace of the superconducting feature with  $T_c$  close to 40 K in samples of nano-dimensional form [34].

It has been a debate whether there exists an antiferromagnetic Mott insulating parent phase, similar to the cuprate superconductors, for FeSe superconductors [35, 36, 37]. Chen et al. first reported the existence of tetragonal  $\beta$ -Fe<sub>1-x</sub>Se with Fe vacancy orders, characterized by analytical transmission electron microscopy [38]. The authors further argued that the Fe<sub>4</sub>Se<sub>5</sub> phase with  $\sqrt{5} \times \sqrt{5}$  Fe-vacancy order to be the parent phase of FeSe superconductors [38]. The Fe vacancy order observed in the Fe<sub>4</sub>Se<sub>5</sub> phase is identical to the Fe-vacancy order observed in the A<sub>2</sub>Fe<sub>4</sub>Se<sub>5</sub> (A=K, Tl, Rb), which has been shown to be an antiferromagnetic [35, 39–42] and is the parent phase of the superconductor A<sub>2-x</sub>Fe<sub>4+x</sub>Se<sub>5</sub> [43, 44]. The detailed studies of the Fe vacancy in K<sub>2</sub>Fe<sub>4+x</sub>Se<sub>5</sub> reveal that its order/disorder is directly associated with superconductivity. A recent study shows that the Fe-vacancy ordered Fe<sub>4</sub>Se<sub>5</sub> nanowire is the non-oxide material with the Verwey-like electronic correlation [45]. It suggests that a charge-ordered state emerges below  $T = 17$  K. The question remains unanswered is whether this Fe-vacancy ordered phase is the parent compound of superconducting FeSe?

In this paper we present the results of structure, electrical transport, and magnetic measurements on the polycrystalline sample of Fe<sub>4</sub>Se<sub>5</sub> treated by rapid-thermal-annealing (RTA) process at a proper temperature and time. After RTA treatment, the sample shows superconductivity with  $T_c \sim 8$  K without changing its chemical stoichiometry. Our findings confirm that the Fe<sub>4</sub>Se<sub>5</sub> with Fe-vacancy order is the parent compound of FeSe superconductors.

## 2 Experimental Techniques

### 2.1 Sample Preparation

Fe<sub>4</sub>Se<sub>5</sub> nanosheets were prepared by a chemical co-precipitation method. First, 200 mL of ethylene glycol was mixed with NaOH and SeO<sub>2</sub> powder and slowly heat up to 160 °C for mixing well.

The volume of 2.4 mL hydrazine hydrate was then added as the reducing agent. Then, at 160 °C, the Fe precursor solution was added and reacted for 12 hours in order to form Fe<sub>4</sub>Se<sub>5</sub> nanosheets. The Fe precursor solution is made by dissolving the amount FeCl<sub>2</sub> in ethylene glycol. The reaction was done under N<sub>2</sub> gas purging to avoid the formation of oxide impurity. To clean the Fe<sub>4</sub>Se<sub>5</sub> nanosheets, the reacted product was dispersed in acetone with absolute ethanol, and high-speed centrifugation is applied to precipitate the nanosheets and remove the capping ligand dissolved in the above organic solvent. The nanosheets were finally dried in vacuum for 24 hours and collected. The process for the rapid thermal annealing (RTA) is: the as-grown Fe<sub>4</sub>Se<sub>5</sub> nanosheets were heated at 450 °C for 10 minutes in a tube furnace with 1atm Ar gas inside to maintain a non-oxidation environment as a rapid thermal treatment process. After the rapid thermal treatment, an air-quenching process was taken by flowing room-temperature Ar gas through the tube. All the samples were stored in the oxygen-free glove box.

## 2.2 Analysis

The crystal structure observation of the Fe<sub>4</sub>Se<sub>5</sub> samples was carried out by the high resolution transmission electron microscope (HRTEM, JEOL JEM-2100F) and 4-circle x-ray diffractometer with the incident beam (12.4 keV) of wavelength 0.82656 Å at beam-line BL13A and wavelength 0.61992 Å at beam-line TPS09A in NSRRC. The temperature-dependent structural information of Fe<sub>4</sub>Se<sub>5</sub> samples was analyzed by the high resolution neutron powder diffraction (high resolution powder diffractometer Echidna with the wavelength of 2.4395 Å at ANSTO). The Fe<sub>4</sub>Se<sub>5</sub> nanosheet powder was pressed into the pallet under 200 kg/cm<sup>2</sup> at 100 °C for 1 hour for the following measurements: To identify the stoichiometry, the energy-disperse X-ray spectrometer (EDS) setup with the SEM (JEOL JSM-7001F Field Emission Scanning Electron Microscope) was applied. To affirm the valence states of the Fe ions, the X-ray photoemission spectroscopy (XPS, VG Scientific ESCALAB 250) measurements for the samples were performed. For polycrystalline bulk samples, the resistance was measured by using the standard four-probe method with silver paste for electrical contact and the Hall measurement by a Hall-bar configuration was done by the Quantum Design Physical Properties Measurement System (PPMS, Model 6000). The magnetic property was measured by the Quantum Design Superconducting quantum interference device (SQUID, VSM).

## 3 Experimental Results and Discussions

### 3.1 Structural analysis of Fe<sub>4</sub>Se<sub>5</sub>

**Figure 1(A)** shows the X-ray diffraction (XRD) patterns of the as-grown Fe<sub>4</sub>Se<sub>5</sub> sample at room temperature. The diffraction pattern, which exhibits superstructure peaks, is refined with a tetragonal *P4* symmetry with  $\sqrt{5}\times\sqrt{5}$  Fe-vacancy order instead of the tetragonal *P4/mmm* symmetry as observed in FeSe [2]. The insets are the TEM image of as-grown Fe<sub>4</sub>Se<sub>5</sub> nanocrystal and its TEM-SAED (selective area electron diffraction) patterns along the *c*-axis. The observation of extra diffraction points among the main diffraction points in the SAED pattern confirms the  $\sqrt{5}\times\sqrt{5}$  Fe-vacancy order in the as-grown Fe<sub>4</sub>Se<sub>5</sub> nanocrystal [35]. After RTA treatment at 450 °C, the superstructure peaks observed in XRD and TEM-SAED due to the  $\sqrt{5}\times\sqrt{5}$  Fe-vacancy order disappears, as shown in **Figure 1(B)** and its inset. The refinement results, using the same *P4* symmetry, reveal that the occupations of Fe at vacancy 4d sites and the originally occupied 16i sites are almost the same, indicating the Fe vacancies becoming disordered after RTA treatment. It is noted that the XRD patterns of the RTA treatment sample show nearly ten times smaller in the intensity response. This is due to the different synchrotron beamlines we used for our measurements. However, the difference does not affect the refined results.

It is noted that the FeSe<sub>4</sub> tetrahedron in as-grown Fe<sub>4</sub>Se<sub>5</sub> is highly distorted due to the existence of the Fe-vacancy order. As the Fe vacancies disordered by the RTA treatment, the FeSe<sub>4</sub> tetrahedron

becomes more symmetric. The refined structure parameters are tabulated in **Supplementary Table 1 and 2**. The EDS analysis confirms that the stoichiometries of samples remain  $\text{Fe}_4\text{Se}_5$  with Fe/Se ratio of 44.5: 55.5 and 45.3: 54.7 before and after the RTA treatment, respectively, as shown in **Supplementary Figure 2** in the supplementary information.

### 3.2 Temperature dependence of the resistance and the magnetic susceptibility measurement of $\text{Fe}_4\text{Se}_5$

**Figure 2(A)** shows the temperature dependence of the resistance for the as-grown polycrystalline pellet sample made of  $\text{Fe}_4\text{Se}_5$  nanosheets. The inset is the magnetic susceptibility of the as-grown sample from 300 K to 2 K. The R-T results of  $\text{Fe}_4\text{Se}_5$  exhibit a metal-insulator transition with the sharp rise in resistance at  $\sim 45$  K. The data can be well-fitted to the three-dimensional Mott variable range hopping model (3D-MVH):  $\rho(T) = \rho_0 \exp(T_0/T)^\nu$ , where  $T_0$  is the variable-range-hopping characteristic temperature, and the exponent  $\nu$  is  $1/(d+1)$  with  $d = 3$ . (The fitting results are shown in **Supplementary Figure 2**. A transition temperature  $T_V$  is marked as the onset temperature of 3D-MVH behavior). The variable-range-hopping characteristic temperature  $T_0$  calculated is  $\sim 1400$  K for the as-grown sample. The magnetic susceptibility of the same sample shows paramagnetic behavior as the sample cools down from 300K, and a sudden drop in susceptibility appears at about the same temperature as the resistance transition temperature ( $T_V$ )  $\sim 45$  K. The sharp resistive rise and the diamagnetic drop are the two signatures for the Verwey transition observed in  $\text{Fe}_3\text{O}_4$ , which occurs at 125K. These results are also in line with those reported results in the  $\text{Fe}_4\text{Se}_5$  nanowire, which was recently demonstrated to exhibit the Verwey-like electronic correlation [45].

**Figure 2(B)** shows the temperature-dependence resistance for the  $\text{Fe}_4\text{Se}_5$  samples after 300 °C and 450 °C RTA process. The sample after 300 °C remains to behave like semiconductor. The sample treated at 450 and 300 °C changes to metallic and becomes superconducting below  $\sim 5$  K with the onset superconductive critical temperature ( $T_c$ )  $\sim 7.8$  K, as evidenced in the upper-left inset of **Figure 2(B)**. The lower-right inset is the magnetic susceptibility, which further demonstrates the superconducting transition with onset  $T_c \sim 7.9$  K. The evolution to superconductivity in this RTA-treated sample is similar to that reported in the  $\text{K}_{2-x}\text{Fe}_{4+y}\text{Se}_5$  system, where superconductivity appears after Fe vacancies becoming disordered through high temperature annealing and rapid quenching processes [43, 44].

### 3.3 XPS and Hall measurement of $\text{Fe}_4\text{Se}_5$

In order to gain more insight into the observed Verwey-like electronic correlation, XPS at room temperature and temperature-dependent Hall measurements on the samples were performed. **Figure 3(A)** is the observed XPS results for the as-grown  $\text{Fe}_4\text{Se}_5$  sample. **Figure 3(A)** is the observed XPS results for the as-grown  $\text{Fe}_4\text{Se}_5$  sample. The XPS spectrum clearly reveals two peaks showing the existence of mixed-valence states of Fe. The observed two peaks, at 708.5 eV and 711.5 eV can be associated with the  $\text{Fe}^{2+}$  and  $\text{Fe}^{3+}$  states, respectively. The best data fitting gives the ratio between  $\text{Fe}^{2+}$  to  $\text{Fe}^{3+}$  close to 1:1. This result is similar to that observed in the magnetite  $\text{Fe}_3\text{O}_4$ .

**Figure 3(B)** displays the XPS results for samples with RTA treated at 300 °C and 450 °C. After the RTA treatment, the  $\text{Fe}^{3+}$  state becomes dominant. The extracted  $\text{Fe}^{3+}$  ion to total Fe atoms ratio is 58.7% for 300 °C RTA-treated and 73.2% for 450 °C RTA-treated samples, respectively, indicating a substantial increase in electron carriers in these samples. It should be noted that the sample after 300 °C still exhibits temperature dependent behavior like semiconductor. No specific difference of Se 3d peak at 54.7 eV before and after the RTA process of the  $\text{Fe}_4\text{Se}_5$  sample according to the XPS result, as shown in **Supplementary Figure 3**.

It is known that tetragonal FeSe is a metal with two-band based on the first-principles electronic structure calculation, for example, by T. Xiang et al., [46]. T. Xiang et al., also reported the electronic structure of Fe<sub>4</sub>Se<sub>5</sub> with  $\sqrt{5} \times \sqrt{5}$  Fe-vacancy order is a pair checkboard antiferromagnetic insulator. The calculation shows the Fe-vacancy ordered Fe<sub>4</sub>Se<sub>5</sub> has a single band structure with n-type carrier dominated and a band gap  $\sim 290$  meV. Berlijn et al., [47] investigated the effect of disordered Fe-vacancies on the normal-state electronic structure of the alkali-intercalated FeSe system, where the KFe<sub>4</sub>Se<sub>5</sub> exhibits exactly the same Fe-vacancy order as that in Fe<sub>4</sub>Se<sub>5</sub>. They found that the disorder of Fe-vacancy can effectively raise the chemical potential giving enlarged electron pockets without adding carriers to the system.

It is noted that as reported by Chen et al. [38], there exists a series of Fe<sub>x</sub>Se<sub>y</sub> compounds with  $x/y = 1/2, 2/3, 3/4, 4/5$ , and etc. We have carried out a systematic study using the co-precipitation method to successfully prepare tetragonal Fe<sub>(1-x)</sub>Se with stoichiometry of Fe<sub>3</sub>Se<sub>4</sub> and Fe<sub>4</sub>Se<sub>5</sub>. Based on the XPS results, the observed Fe<sup>3+</sup>/Fe<sup>2+</sup> ratio is 2 and 1 for tetragonal Fe<sub>3</sub>Se<sub>4</sub> and Fe<sub>4</sub>Se<sub>5</sub>, respectively, as shown in **Supplementary Figure 4 (A)** and **Figure 3 (A)**. These data imply that Fe<sub>3</sub>Se<sub>4</sub> would be hole-doped and Fe<sub>4</sub>Se<sub>5</sub> be electron-doped if there are additional carriers based on the simple charge balance picture by considering Fe<sub>3</sub>Se<sub>4</sub> to be the combination of Fe<sup>(2+)</sup>Se and Fe<sub>2</sub><sup>(3+)</sup>Se<sub>3</sub>, whereas Fe<sub>4</sub>Se<sub>5</sub> is from 2(Fe<sup>(2+)</sup>Se) and Fe<sub>2</sub><sup>(3+)</sup>Se<sub>3</sub>. Indeed, our Hall measurement results show at 300 K a hole concentration of  $1.20 \times 10^{19}/\text{cm}^3$  for Fe<sub>3</sub>Se<sub>4</sub> (**Supplementary Figure 4(B)**) and electron concentration of  $-6.52 \times 10^{17}/\text{cm}^3$  for Fe<sub>4</sub>Se<sub>5</sub>.

Both of the as grown and RTA treated Fe<sub>4</sub>Se<sub>5</sub> show a single-band behavior with n-type carrier from the Hall resistivity measurements, as shown in **Supplementary Figure 5**. The Hall coefficient of the as-grown sample at room temperature is  $-9.59 \text{ cm}^3/\text{C}$ , corresponding to the electron carrier concentration of  $6.52 \times 10^{17} \text{ cm}^{-3}$ , and the carrier concentration decreases by about a factor of 8 at the transition temperature  $T_v$ , as shown in **Figure 3(C)**.

After the Fe<sub>4</sub>Se<sub>5</sub> sample is RTA-treated at 450 °C, the Fe<sup>3+</sup>/Fe<sup>2+</sup> ratio becomes close to 3:1, which means a large number of electrons are introduced, and subsequently induced superconductivity. Indeed, the Hall measurement results, as shown in **Figure 3(D)**, show that the carrier concentration at 300 K increases to  $-3.34 \times 10^{21}/\text{cm}^3$  (Hall coefficient  $-1.87 \times 10^{-3} \text{ cm}^3/\text{C}$ ) for 450 °C RTA-treated sample. The electron carrier concentration is about four orders of magnitude increase comparing with the as-grown Fe<sub>4</sub>Se<sub>5</sub>. Obviously, the RTA treatment disrupts the Fe-vacancy long-range order and leads to the increase of electron carriers.

### 3.4 Neutron diffraction of Fe<sub>4</sub>Se<sub>5</sub>

It is well known that the Verwey transition in magnetite exhibits a structural transition accompanying with the sharp resistive and magnetic susceptibility changes. To examine whether such a structural change exists for the as-grown Fe<sub>4</sub>Se<sub>5</sub>, we have carried out the neutron diffraction at low temperatures.

The detailed structural information of the as-grown Fe<sub>4</sub>Se<sub>5</sub> sample measured by neutron diffraction at different temperatures is shown in **Figure 4**. At room temperature, the neutron data, consistent with XRD results, fit well with the *P4*-tetragonal symmetry. At low temperatures, a distortion appears at temperatures below 30K. The data at 5 K, with an evident peak emerge shown in the inset of **Figure 4**, indicates a possible structural change. This result further supports that the as-grown Fe<sub>4</sub>Se<sub>5</sub> nanosheets, similar to the results observed in Fe<sub>4</sub>Se<sub>5</sub> nanowire, shows the Verwey-like correlation. The Verwey-like transition temperature of  $\sim 45$  K in nanosheets is higher than that observed in the nanowire, which was found to be  $\sim 30$  K. This shows the size dependence of  $T_v$ , which also

noticed in Verwey transition [48-50]. Currently, we are waiting for the results of the detailed high-resolution XRD at low temperatures using a synchrotron source to determine exactly the low-temperature phase and the transition temperature.

## 4 Conclusions

We have carried out a detailed study to investigate whether there exists an insulating parent phase for FeSe superconductor. Our studies unambiguously show that: (1) the  $\sqrt{5} \times \sqrt{5}$  Fe-vacancy ordered Fe<sub>4</sub>Se<sub>5</sub> a Mott insulator with Verwey-like transition at low temperature; (2) Fe<sub>4</sub>Se<sub>5</sub> is the parent compound of the FeSe superconductors. The application of the RTA process at 450 °C disrupts Fe-vacancy order and induces more electron carriers by increasing the Fe<sup>3+</sup> valence state. Superconductivity emerges with  $T_c \sim 8$  K without changing the chemical stoichiometry of the sample after the RTA process. Consistent with the observations in K<sub>2</sub>Fe<sub>4+x</sub>Se<sub>5</sub>, superconductivity is directly related to the disappearance of Fe-vacancy long-range order. In the Fe<sub>4</sub>Se<sub>5</sub> case, no extra Fe doping is required as the random occupation of Fe atom in the vacancy sites, resulting in the addition of extra carriers in favor of superconductivity. More detailed evolution of superconductivity by varying the RTA temperature and time is currently underway in order to gain more insight into the exact phase diagram of the FeSe superconductors.

## 5 Author Contributions

M.-J.W., and M.-K.W. designed research. K.-Y.Y., T.-S.L., and Y.-R. C. performed research. M.-J.W. and K.-S.C.-L. contributed new reagents/analytic tools. K.-Y.Y., T.-S.L., P.M.W., Y.-R. C., K.-S.C.-L., M.-J.W., and M.-K.W. analyzed data and took part in physics discussions. K.-Y.Y., M.-J.W., T.-S.L., P.M.W. and M.-K.W. wrote the paper.

## 6 Funding

The work is supported by the Ministry of Science and Technology under Grant No. MOST108-2633-M-001-001 and Academia Sinica Thematic Research Grant No. AS-TP-106-M01.

## 7 Acknowledgments

The authors appreciate very much the help from Dr. G.T Huang for synchrotron XRD measurements, and Dr. C.P. Yen for the analysis of XPS results. We thank the technical support from NanoCore, the Core Facilities for Nanoscience and Nanotechnology at Academia Sinica in Taiwan.

## 8 Conflict of Interest

The authors declare that the research was conducted in the absence of any commercial or financial relationships that could be construed as a potential conflict of interest.

## 9 Copy rights

Keng-Yu Yeh, Yan-Rai Chen, Tung-Sheng Lo, Phillip M. Wu, Ming-Jye Wang, Kuei-Shu Chang-Liao, and Maw-Kuen Wu. This is an open-access article distributed under the terms of the Creative Commons Attribution License (CC BY). The use, distribution or reproduction in other forums is permitted, provided the original author(s) and the copyright owner(s) are credited and that the original publication in this journal is cited, in accordance with accepted academic practice. No use, distribution or reproduction is permitted which does not comply with these terms.

## 10 References

1. Kamihara Y, Watanabe T, Hirano M, Hosono H. Iron-Based Layered Superconductor  $\text{La}[\text{O}_{1-x}\text{F}_x]\text{FeAs}$  ( $x = 0.05-0.12$ ) with  $T_c = 26$  K. *J. Am. Chem. Soc.* (2008) **130**: 3296. doi:10.1021/ja800073m
2. Hsu FC, Luo JY, Yeh KW, Chen TK, Huang TW, Wu PM, Lee YC, Huang YL, Chu YY, Yan DC, Wu MK. Superconductivity in the PbO-type structure  $\alpha$ -FeSe. *Proc. Natl. Acad. Sci. U.S.A.* (2008) **105**:14262. doi: 10.1073/pnas.0807325105
3. Peng R, Xu HC, Tan SY, Cao H, Xia M, Shen XP, Huang Z, Wen CHP, Song Q, Zhang T, Xie BP, Gong XG, Feng DL. Tuning the band structure and superconductivity in single-layer FeSe by interface engineering, *Nat. Commun.* (2014) **5**:5044 EP. doi: 10.1038/ncomms6044
4. Yi M, Zhang Y, Shen ZX, Lu D. Role of the orbital degree of freedom in iron-based Superconductors, *npj Quantum Materials* (2017) **2**:57. doi:10.1038/s41535-017-0059-y
5. Fernandes RM, Chubukov AV, Schmalian J. Magnetically driven suppression of nematic order in an iron-based superconductor. *Nat. Phys.* (2014) **10**: 97. doi:10.1038/NPHYS2877
6. Yu R, Zhu JX, Si Q. Orbital selectivity enhanced by nematic order in FeSe, *Phys. Rev. Lett.* (2018) **121**: 227003. doi:10.1103/PhysRevLett.121.227003
7. Saito T, Onari S, Kontani H. Orbital fluctuation theory in iron pnictides: Effects of As-Fe-As bond angle, isotope substitution, and  $Z_2$ -orbital pocket on superconductivity. *Phys. Rev. B* (2010) **82**: 144510. doi: 10.1103/PhysRevB.82.144510
8. Kontani H, Onari S. Orbital-fluctuation-mediated superconductivity in iron pnictides: analysis of the five-orbital Hubbard-Holstein model, *Phys. Rev. Lett.* (2010) **104**:157001. doi: 10.1103/PhysRevLett.104.157001
9. Yu W, Aczel AA, Williams TJ, Bud'ko SL, Ni N, Canfield PC, Luke GM. Absence of superconductivity in single-phase  $\text{CaFe}_2\text{As}_2$  under hydrostatic pressure. *Phys. Rev. B* (2009) **79**:020511(R). doi: 10.1103/PhysRevB.79.020511
10. Goldman AI, Argyriou DN, Ouladdiaf B, Chatterji T, Kreyssig A, Nandi S, Ni N, Budko SL, Canfield PC, McQueeney RJ. Lattice and magnetic instabilities in  $\text{CaFe}_2\text{As}_2$ : A single-crystal neutron diffraction study. *Phys. Rev. B* (2008) **78**: 100506 R. doi: 10.1103/PhysRevB.78.100506
11. Margadonna S, Takabayashi Y, McDonald MT, Kasperkiewicz K, Mizuguchi Y, Takano Y, Fitch AN, Prassides K SE. Crystal structure of the new  $\text{FeSe}_{1-x}$  superconductor. *Chem. Commun.* (2008) **0**:5607. doi: 10.1039/b813076k
12. McQueen TM, Williams AJ, Stephens PW, Tao J, Zhu Y, Ksenofontov V, Casper F, Felser C and Cava RJ. Tetragonal-to-orthorhombic structural phase transition at 90 K in the superconductor  $\text{Fe}_{1.01}\text{Se}$ . *Phys. Rev. Lett.* (2009) **103**:057002. doi: 10.1103/PhysRevLett.103.057002
13. Bendele M, Amato A, Conder K, Elender M, Keller H, Klauss H-H, Luetkens H, Pomjakushina E, Raselli A, Khasanov R. Pressure induced static magnetic order in superconducting  $\text{FeSe}_{1-x}$ . *Phys. Rev. Lett.* (2010) **104**: 087003. doi: 10.1103/PhysRevLett.104.087003
14. Baek SH, Efremov DV, Ok JM, Kim JS, Brink JVD, Bchner B. Orbital-driven nematicity in FeSe. *Nat. Mater.* (2015) **14**:210. doi: 10.1038/NMAT4138
15. Bohmer AE, Arai T, Hardy F, Hattori T, Iye T, Wolf T, Lohneysen HV, Ishida K, Meingast C. Origin of the Tetragonal-to-Orthorhombic Phase Transition in FeSe:A Combined Thermodynamic and NMR Study of Nematicity. *Phys. Rev. Lett.* (2015) **114**: 027001. doi: 10.1103/PhysRevLett.114.027001

16. Chubukov AV, Fernandes RM, Schmalian J. Origin of nematic order in FeSe. *Phys. Rev. B* (2015) **91**:201105. doi: 10.1103/PhysRevB.91.201105
17. Glasbrenner JK, Mazin II, Jeschke HO, Hirschfeld PJ, Fernandes RM, Valentí R. Effect of magnetic frustration on nematicity and superconductivity in iron chalcogenides. *Nat. Phys.* (2015) **11**:953. doi: 10.1038/NPHYS3434
18. Wang F, Kivelson SA, Lee DH. Nematicity and quantum paramagnetism in FeSe.(2015). *Nat. Phys.* **11**, 959. doi: 10.1038/NPHYS3456
19. Yu R, Si QM. Antiferroquadrupolar and Ising-Nematic Orders of a Frustrated Bilinear-Biquadratic Heisenberg Model and Implications for the Magnetism of FeSe. *Phys. Rev. Lett.* (2015)**115**:116401. doi: 10.1103/PhysRevLett.115.116401
20. Wang QS, Shen Y, Pan BY, Hao YO, Ma MW, Zhou F, Steffens P, Schmalzl K, Forrest TR, Abdel-Hafiez M, Chen XJ, Chareev DA, Vasiliev AN, Bourges P, Sidis Y, Cao HB, Zhao J. Strong interplay between stripe spin fluctuations, nematicity and superconductivity in FeSe. *Nat. Mater.* (2016) **15**: 159. doi: 10.1038/NMAT4492
21. Bendele M, Ichsanow A, Pashkevich Y, Keller L, Strassle T, Gusev A, Pomjakushina E, Conder K, Khasanov R, Keller H. Coexistence of superconductivity and magnetism in FeSe<sub>1-x</sub> under pressure. *Phys. Rev. B* (2012). **85**: 064517. doi: 10.1103/PhysRevB.85.064517
22. Mizuguchi Y, Tomioka F, Tsuda S, Yamaguchi T, Takano Y. Superconductivity at 27 K in tetragonal FeSe under high pressure. *Appl. Phys. Lett.* (2008). **93**: 152505. doi: 10.1063/1.3000616
23. Medvedev S et al.. Electronic and magnetic phase diagram of  $\beta$ -Fe<sub>1.01</sub> with superconductivity at 36.7 K under pressure. *Nat. Mater.* (2009)**8**: 630. doi: 10.1038/NMAT2491
24. Margadonna S, Takabayashi Y, Ohishi Y, Mizuguchi Y, Takano Y, Kagayama T, Nakagawa T, Takata M, Prassides K. Pressure evolution of the low-temperature crystal structure and bonding of the superconductor FeSe ( $T_c = 37$  K). *Phys. Rev. B* (2009). **80**: 064506. doi: 10.1103/PhysRevB.80.064506
25. Garbarino G, Sow A, Lejay P, Sulpice A, Toulemonde P, Mezouar M, Nunez-Regueiro M. High-temperature superconductivity ( $T_c$  onset at 34 K) in the high-pressure orthorhombic phase of FeSe. *Europhys. Lett.* (2009) **86** 27001. doi: 10.1209/0295-5075/86/27001
26. Masaki S, Kotegawa H, Hara Y, Tou H, Murata K, Mizuguchi Y, Takano Y. Precise pressure dependence of the superconducting transition temperature of FeSe: resistivity and <sup>77</sup>Se-NMR study. *J. Phys. Soc. Japan* (2009).**78**: 063704. doi: 10.1143/JPSJ.78.063704
27. Okabe H, Takeshita N, Horigane K, Muranaka T, Akimitsu J. Pressure-induced high- $T_c$  superconducting phase in FeSe: correlation between anion height and  $T_c$ . *Phys. Rev. B* (2010).**81**:205119. doi: 10.1103/PhysRevB.81.205119
28. Wang QY, Li Z, Zhang WH, Zhang ZC, Zhang JS, Li W, Ding H, Ou YB et al..Interface-induced high-temperature superconductivity in single unit-cell FeSe films on SrTiO<sub>3</sub>. *Chin. Phys. Lett.* (2012) **29**: 037402. doi: 10.1088/0256-307X/29/3/037402
29. Liu DF, Zhang WH, Mou DX, He JF, Ou YB et al.. Electronic origin of high-temperature superconductivity in single-layer FeSe superconductor. *Nat. Commun.* (2012) **3**:931. doi: 10.1038/ncomms1946
30. He SL, He JF, Zhang WH, Zhao L, Liu DF et al.. Phase diagram and electronic indication of high-temperature superconductivity at 65 K in single-layer FeSe films. *Nat. Mater.* (2013) **12**: 605. doi: 10.1038/NMAT3648



31. Tan SY, Zhang Y, Xia M, Ye ZR, Chen F et al.. Interface-induced superconductivity and strain-dependent spin density waves in FeSe/SrTiO<sub>3</sub> thin films. *Nat. Mater.* (2013) **12**: 634. doi: 10.1038/NMAT3654
32. McQueen TM, Huang Q, Ksenofontov V, Felser C, Xu Q, Zandbergen H et al.. Extreme sensitivity of superconductivity to stoichiometry in Fe<sub>1+δ</sub>Se. *Phys. Rev. B* (2009) **79**(1):014522. doi: 10.1103/PhysRevB.79.014522
33. Liu TJ, Hu J, Qian B, Fobes D, Mao ZQ, Bao W et al.. From (π,0) magnetic order to superconductivity with (π,π) magnetic resonance in Fe<sub>1.02</sub>Te<sub>1-x</sub>Se<sub>x</sub>. *Nat. Mater.* (2010) **9**:718. doi: 10.1038/NMAT2800
34. Chang CC, Wang CH, Wen MH, Wu YR, Hsieh YT, Wu MK. Superconductivity in PbO-type tetragonal FeSe nanoparticles. *Solid State Commun.*(2012) **152**:649.doi: 10.1016/j.ssc.2012.01.030
35. Zhou Y, Xu DH, Zhang FC, Chen WQ. Theory for superconductivity in (Tl,K)Fe<sub>x</sub>Se<sub>2</sub> as a doped Mott insulator, *Europhys. Lett.* (2011) **95**: 17003. doi: 10.1209/0295-5075/95/17003
36. Yu R, Zhu JX, Si Q. Mott Transition in Modulated Lattices and Parent Insulator of (K; Tl)<sub>y</sub>Fe<sub>x</sub>Se<sub>2</sub> Superconductors, *Phys. Rev. Lett.* (2011) **106**:186401. doi: 10.1103/PhysRevLett.106.186401
37. Zhao X, Ma F, Lu ZY, Xiang T. AFeSe<sub>2</sub> (A = Tl, K, Rb, or Cs): Iron-based superconducting analog of the cuprates, *Phys. Rev. B* (2020) **101**: 184504. doi: 10.1103/PhysRevB.101.184504
38. Chen TK, Chang CC, Chang HH, Fang AH, Wang CH, Chao WH, Tseng CM, Lee YC, Wu YR, Wen MH, Tang HY, Chen FR, Wang MJ, Wu MK, Van Dyck D. Fe-vacancy order and superconductivity in tetragonal β-Fe<sub>1-x</sub>Se. *Proc. Natl. Acad. Sci. U.S.A.* (2014) **111**: 63. doi: 10.1073/pnas.1321160111
39. Bao W, Huang QZ, Chen GF, Green MA, Wang DM, He JB, Qiu YM. A novel large moment antiferromagnetic order in K<sub>0.8</sub>Fe<sub>1.6</sub>Se<sub>2</sub> superconductor, *Chin. Phys. Lett.* (2011) **28**: 086104. doi: 10.1088/0256-307X/28/8/086104
40. Zhao J, Cao H, Bourret-Courchesne E, Lee DH, Birgeneau RJ. Neutron-diffraction measurements of an antiferromagnetic semiconducting phase in the vicinity of the high-temperature superconducting state of K<sub>x</sub>Fe<sub>2-y</sub>Se<sub>2</sub>, *Phys. Rev. Lett.* (2012) **109**: 267003. doi: 10.1103/PhysRevLett.109.267003
41. Liu RH, Luo XG, Zhang M, Wang AF, Ying JJ, Wang XF, Yan YJ, Xiang ZJ, Cheng P, Ye GJ, Li ZY, Chen XH, Coexistence of superconductivity and antiferromagnetism in single crystals A<sub>0.8</sub>Fe<sub>2-y</sub>Se<sub>2</sub> (A = K, Rb, Cs, Tl/K and Tl/Rb): Evidence from magnetization and resistivity, *Europhys. Lett.* (2011) **94**: 27708. doi: 10.1209/0295-5075/94/27708
42. Fang MH, Wang HD, Dong CH, Li ZJ, Feng CM, Chen J, Yuan HQ, Fe-based superconductivity with T<sub>c</sub> = 31 K bordering an antiferromagnetic insulator in (Tl,K) Fe<sub>x</sub>Se<sub>2</sub>, *Europhys. Lett.* (2011) **94**: 27009. doi: 10.1209/0295-5075/94/27009
43. Wang CH, Chen TK, Chang CC, Hsu CH, Lee YC, Wang MJ, Wu PM, Wu MK. Disordered Fe vacancies and superconductivity in potassium-intercalated iron selenide (K<sub>2-x</sub>Fe<sub>4+y</sub>Se<sub>5</sub>). *Europhys. Lett.* (2015) **111**: 27004. doi: 10.1209/0295-5075/111/27004
44. Wang CH, Lee CC, Huang GT, Yang JY, Wang MJ, Sheu HS, Lee JJ, Wu MK. Role of the extra Fe in K<sub>2-x</sub>Fe<sub>4+y</sub>Se<sub>5</sub> superconductors. *Proc. Natl. Acad. Sci. U.S.A.* (2019) **116**:1104. doi: 10.1073/pnas.1815237116
45. Yeh KY, Lo TS, Wu PM, Chang-Liao KS, Wang MJ, Wu MK. Magneto-transport studies of Fe-Vacancy Ordered Fe<sub>4+δ</sub>Se<sub>5</sub> Nanowires. *Proc. Natl. Acad. Sci. U.S.A.* (2020) **116**:1104. doi: 10.1073/pnas.2000833117

46. Ma F, Ji W, Hu JP, Lu ZY, Xian T. First-Principles Calculations of the Electronic Structure of Tetragonal  $\alpha$ -FeTe and  $\alpha$ -FeSe Crystals: Evidence for a Bicollinear Antiferromagnetic Order. *Phys. Rev. Lett.* (2009) **102**:177003 doi: 10.1103/PhysRevLett.102.177003
47. Berlijn T, Hirschfeld PJ, Ku W. Effective Doping and Suppression of Fermi Surface Reconstruction via Fe Vacancy Disorder in  $K_xFe_{2-y}Se_2$ . *Phys. Rev. Lett.* (2012) **109**:47003 w, doi:10.1103/PhysRevLett.109.147003
48. Zisese M, Blythe HJ. Magnetoresistance of magnetite. *J.Phys.:condens. Matter* (2000) **13**:12. doi: 10.1088/0953-8984/12/1/302
49. M Bohra, Agarwal N, Sigh V. A short review on Verwey transition in nanostructured  $Fe_3O_4$  materials. *J. Nanomater.* (2019).**18**:doi: 10.1155/2019/8457383
50. Kim T, Lim S, Hong J, Kwon SG, Okamoto J et al.. Giant thermal hysteresis in Verwey transition of single domain  $Fe_3O_4$  nanoparticles, *Sci. Rep.* (2018) **8**: 5092. doi: 10.1038/s41598-018-23456-6

## 11 Figures

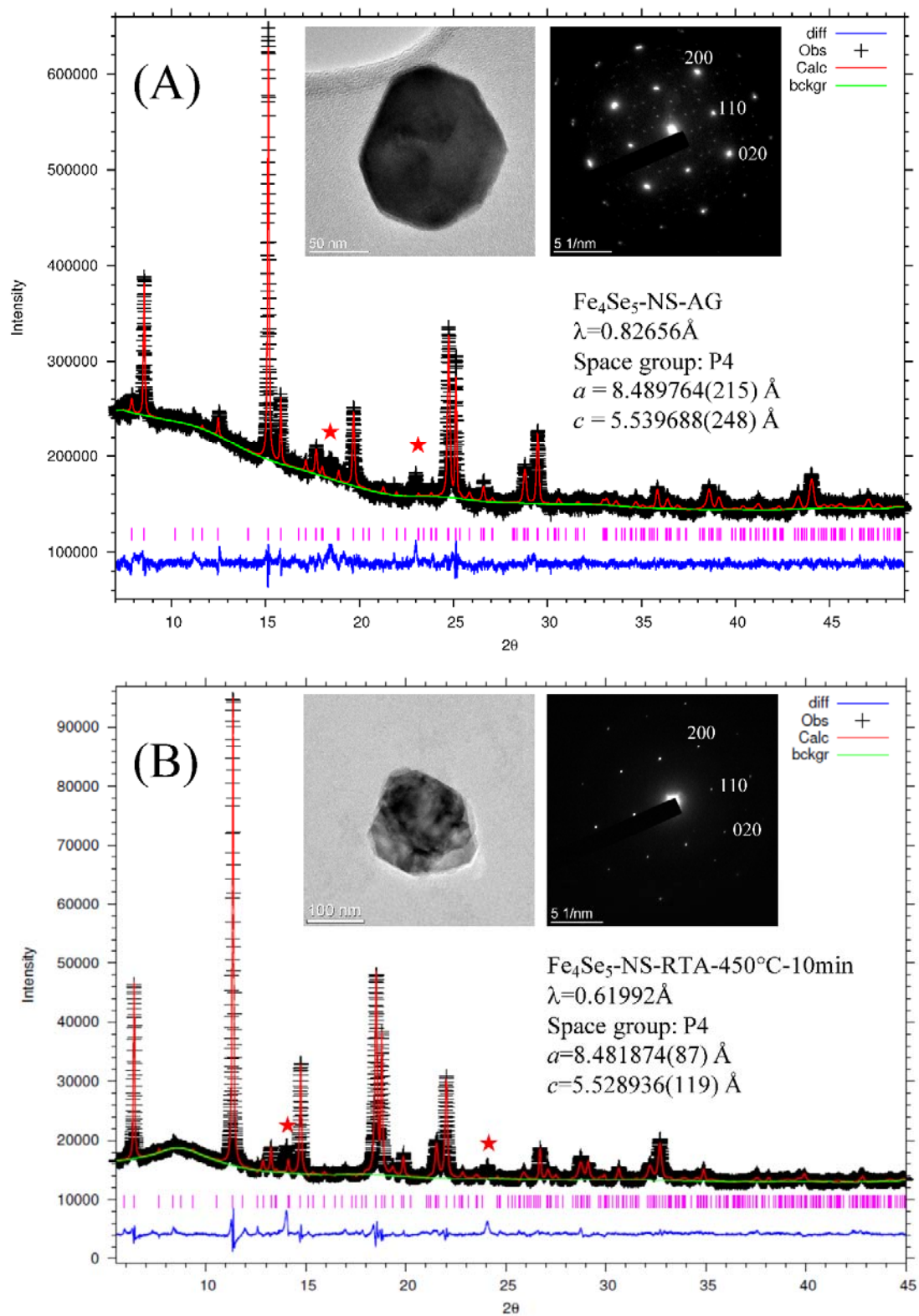


**Figure 1.** X-ray diffraction patterns and their Reitveld refinement results of (A) the as-grown  $\text{Fe}_4\text{Se}_5$  nanocrystals and (B) the sample after the RTA process at 450 °C. The insets in (A) and (B) show the

transmission electron microscope (TEM) images and selective area electron diffraction (SAED) patterns of the samples, respectively.

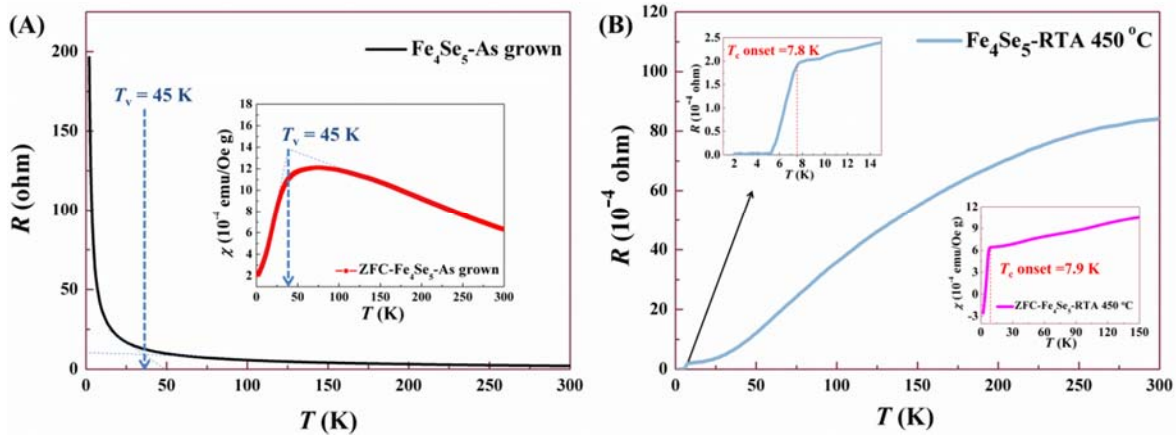


**Figure 2.** (A) Temperature-dependent resistance of the as-grown  $\text{Fe}_4\text{Se}_5$  sample showing a metal-insulator transition  $T_v$  with the onset of resistance rise at  $\sim 45$  K. The inset is the magnetic susceptibility from 300 K to 2 K of the same sample, which shows a large drop in susceptibility with the onset temperature also at  $\sim 45$  K. (B) Temperature-dependent resistance of the  $\text{Fe}_4\text{Se}_5$  sample after 450 °C RTA process. The sample becomes metallic and shows superconducting transition with the onset  $T_c \sim 7.8$  K, as highlighted in the upper-left inset. The lower-right inset is the magnetic susceptibility further demonstrates the superconducting transition with  $T_c \sim 7.9$  K.

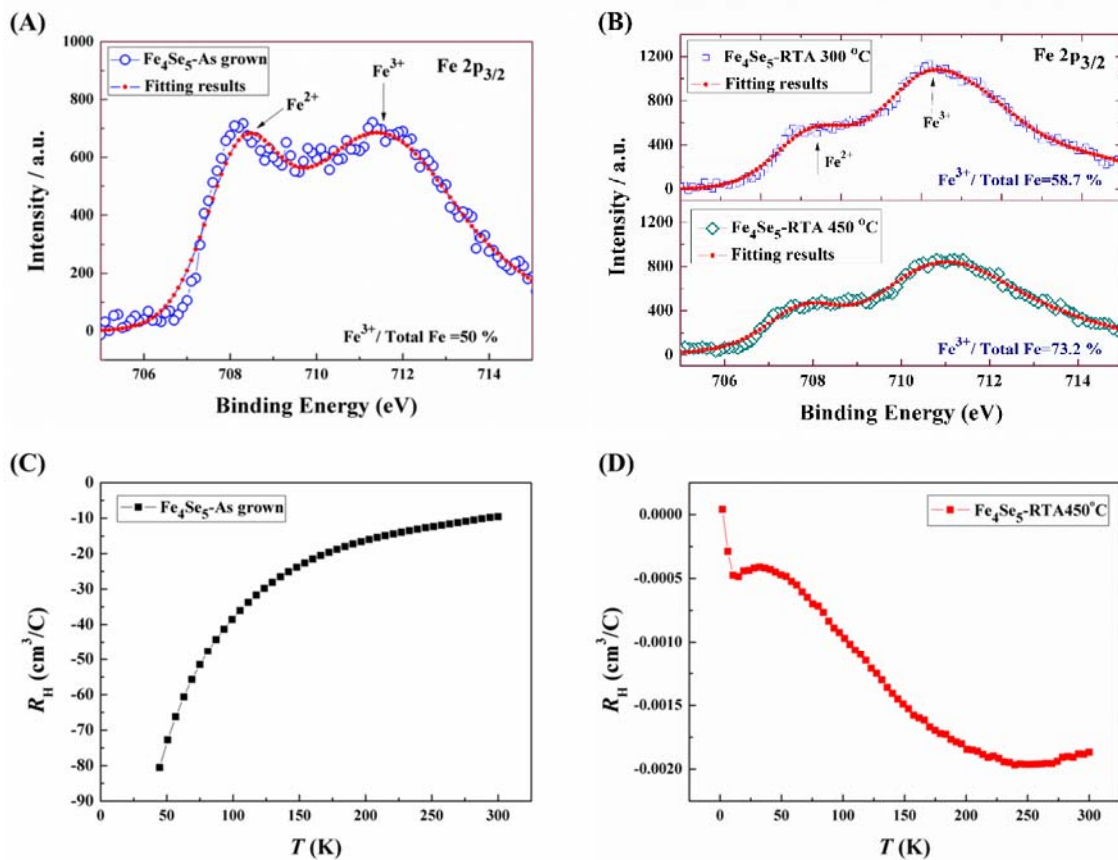


**Figure 3.**  $\text{Fe}_{2p_{3/2}}$  spectrum of XPS analysis for (A) the as-grown  $\text{Fe}_4\text{Se}_5$  sample and (B) the 300 °C and 450 °C RTA-treated  $\text{Fe}_4\text{Se}_5$  sample. The temperature dependent Hall coefficient for (C) the as-grown  $\text{Fe}_4\text{Se}_5$  sample and (D) the 450 °C RTA-treated  $\text{Fe}_4\text{Se}_5$  sample.

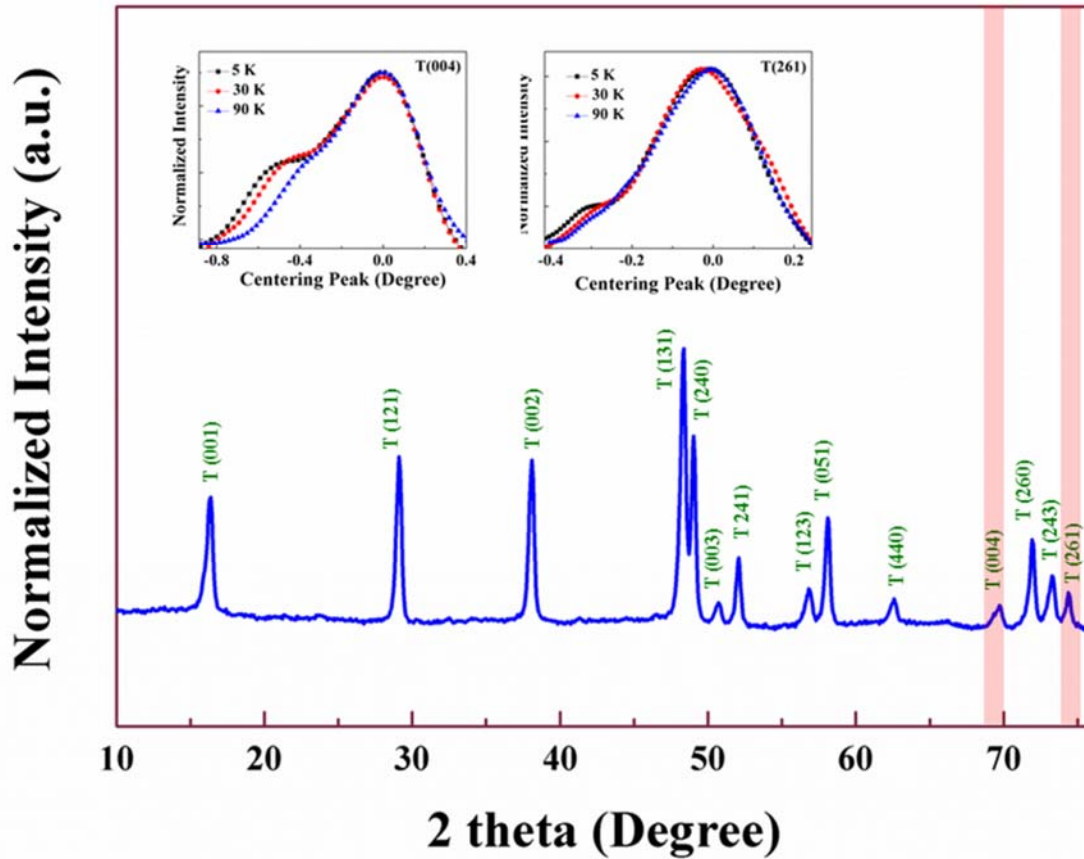
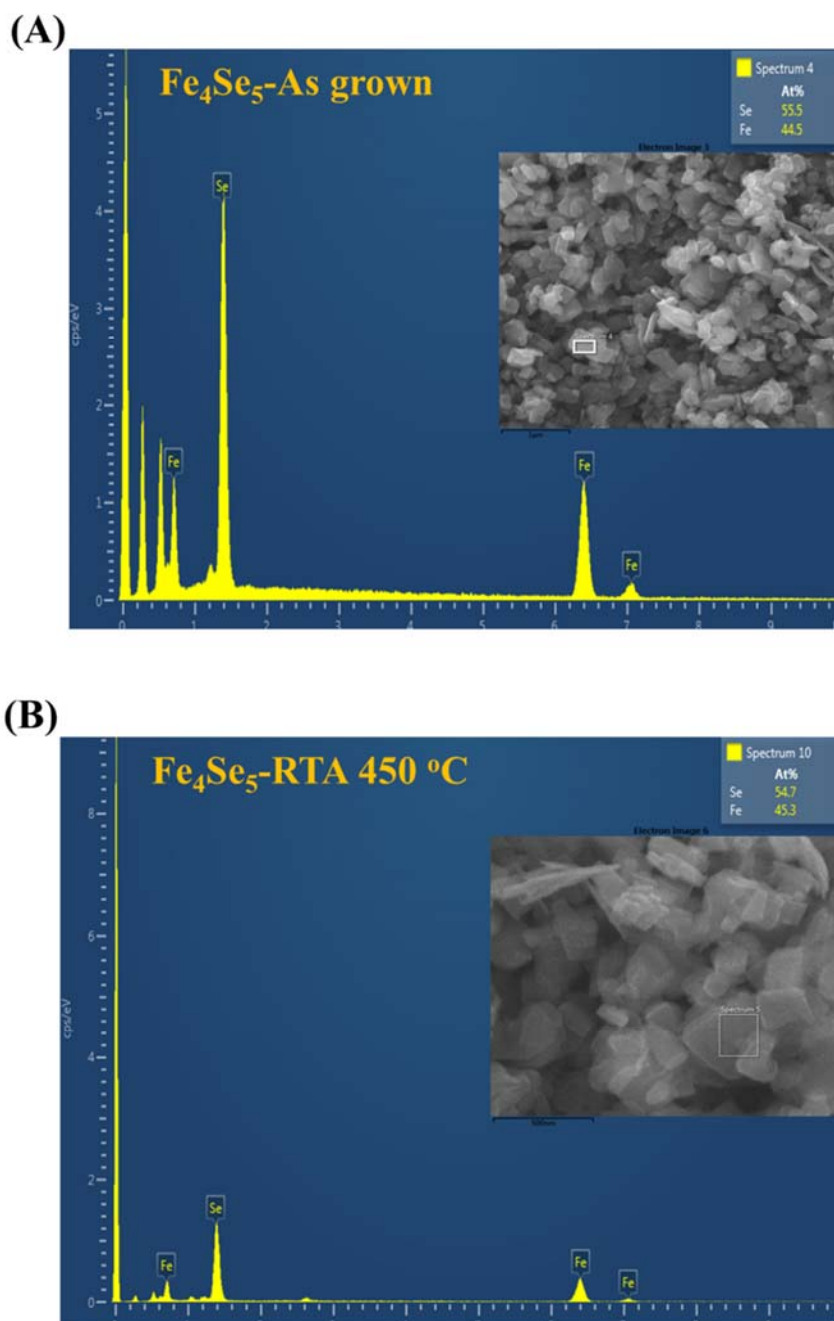
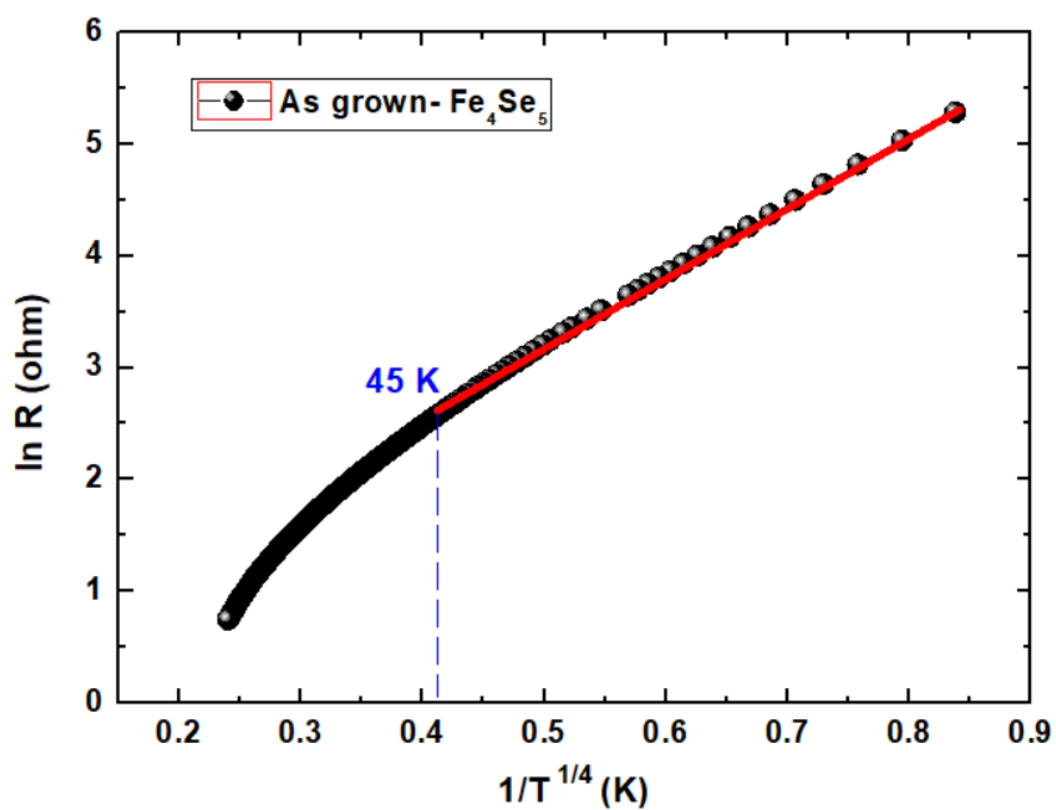


**Figure 4.** The neutron diffraction patterns of as-grown  $\text{Fe}_4\text{Se}_5$  nanosheet at 300\_K, the tetragonal  $P4$  symmetry is identified. The insets are the diffraction peaks of (004) and (261) at low temperatures showing the growth of additional peaks, indicating a structural change at low temperature.

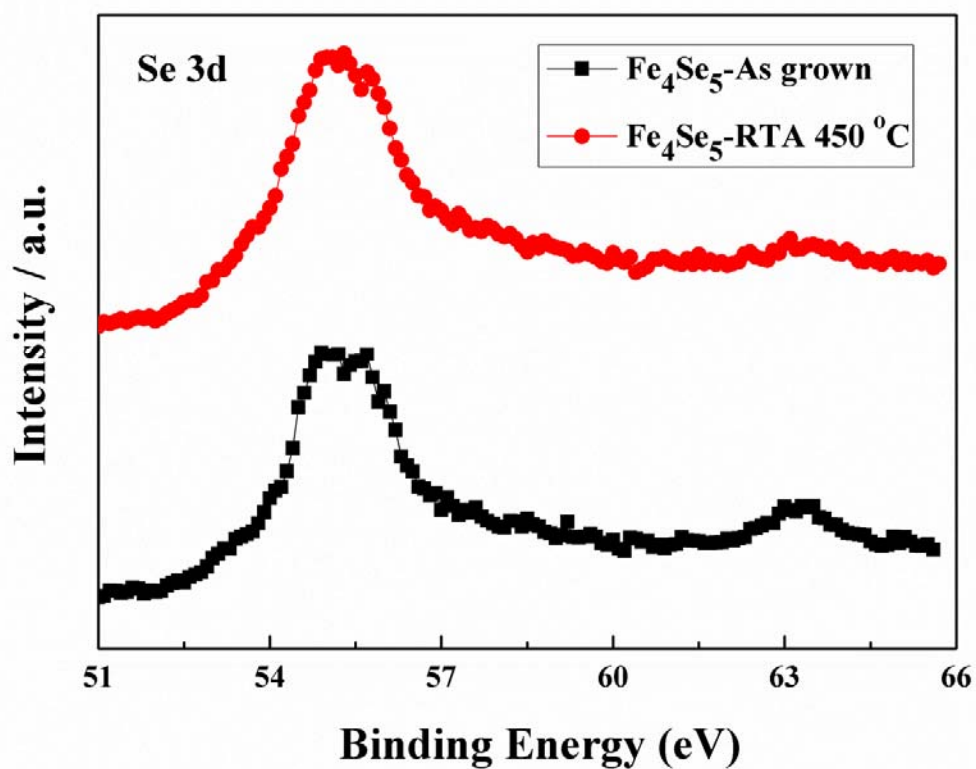
## Supplementary Material



**Supplementary Figure 3.** The EDS spectrums of (A) the as-grown Fe<sub>4</sub>Se<sub>5</sub> sample and (B) the RTA-treated Fe<sub>4</sub>Se<sub>5</sub> sample.



**Supplementary Figure 2.** Natural logarithmic resistance plotted against  $1/T^{1/4}$  for the as grown  $\text{Fe}_4\text{Se}_5$ , in which the data between 2 and 45 K fit nicely by the 3D Mott variable range hopping model.



**Supplementary Figure 3.** (A) Se<sub>3d</sub> spectrums of XPS analysis for the as-grown Fe<sub>4</sub>Se<sub>5</sub> sample and the RTA-treated Fe<sub>4</sub>Se<sub>5</sub> sample.

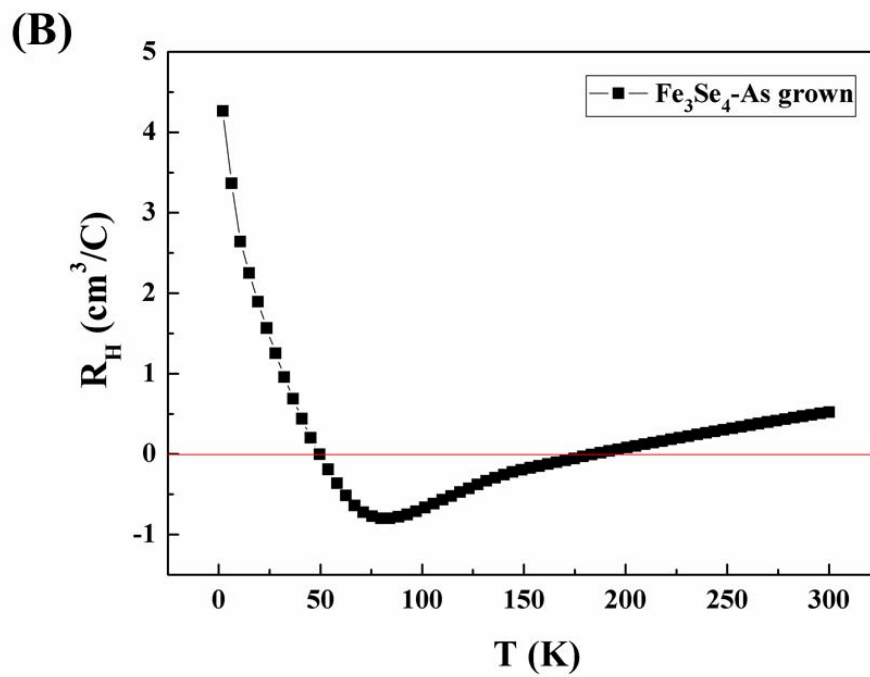
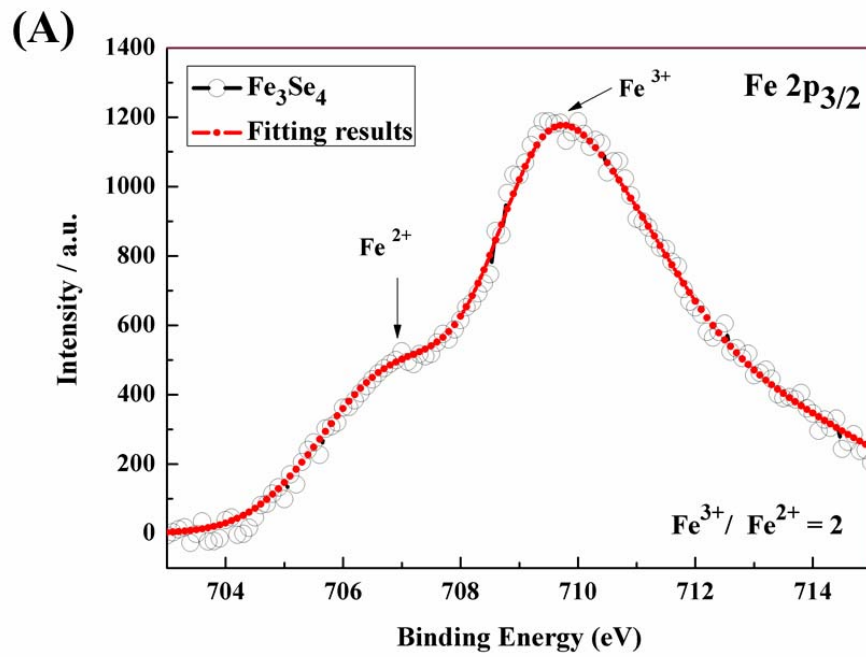


Space group: P4, wRp=0.0273, Rp=0.0215, $\chi^2=74.32$				
$a=8.489764(215)$ Å, $c=5.539688(248)$ Å				
	<i>x</i>	<i>y</i>	<i>z</i>	<i>F</i>
Fe-vacancy	0.5	0	0	0
Fe1	0.231613(405)	0.084124(474)	0.003925(2238)	1
Fe2	0.304264(476)	0.427243(519)	0.008273(2553)	1
Se1	0.199810(270)	0.580714(251)	0.259196(740)	1
Se2	0.079586(316)	0.301426(291)	0.743104(000)	1
Se3	0.5	0.5	0.703410(2183)	1
Se4	0	0	0.262407(2349)	1

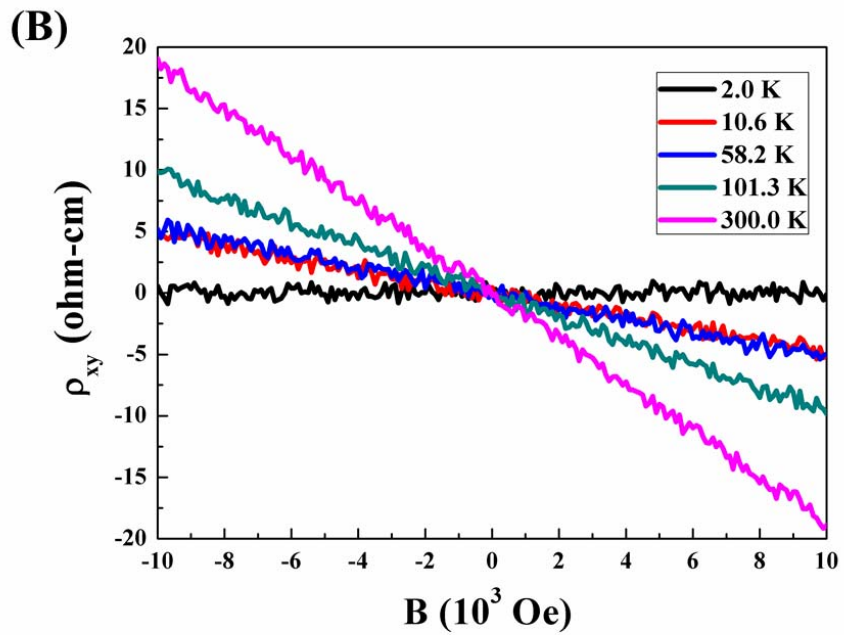
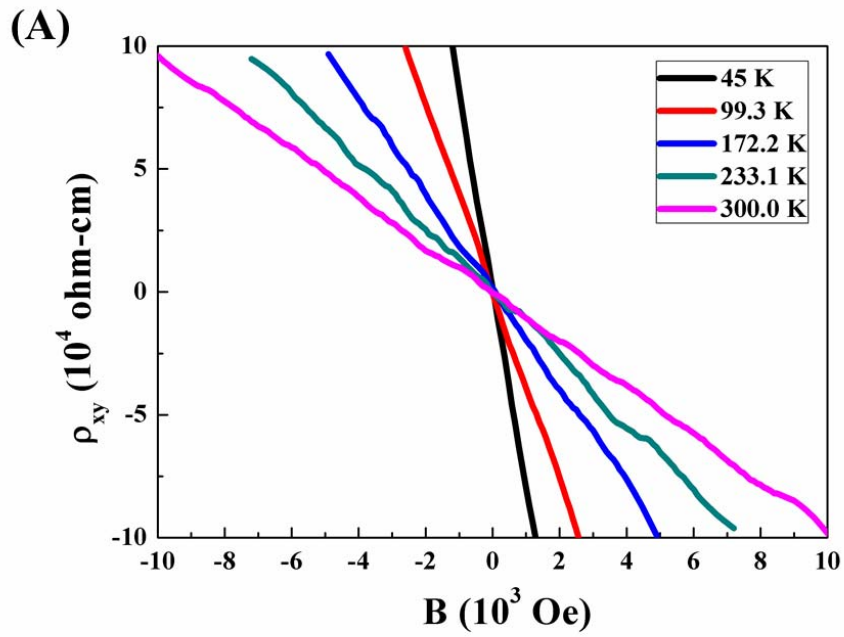
**Supplementary Table 1.** The structure parameters of as-grown Fe<sub>4</sub>Se<sub>5</sub> samples as Rietveld refinement from synchrotron diffraction data.

Space group: P4 symmetry, wRp=0.0366, Rp=0.0267, $\chi^2=8.613$				
$a= 8.481874(87) \text{ \AA}$ , $c= 5.528936(119) \text{ \AA}$				
	$x$	$y$	$z$	$F$
Fe-vacancy	0.5	0	-0.002332(6026)	0.806(5)
Fe1	0.200949(354)	0.099602(275)	0.003730(6082)	0.776(3)
Fe2	0.301253(347)	0.397302(259)	-0.007367(5753)	0.847(3)
Se1	0.199458(226)	0.597664(141)	0.268049 (4531)	1
Se2	0.098462(150)	0.299195(200)	0.745687(4541)	1
Se3	0.5	0.5	0.740596(4441)	1
Se4	0	0	0.259767(4405)	1

**Supplementary Table 2.** The structure parameters of RTA-treated Fe<sub>4</sub>Se<sub>5</sub> samples.



**Supplementary Figure 4.** (A) Fe<sub>2p<sub>3/2</sub></sub> spectrum of XPS analysis and (B) the temperature dependent Hall coefficient for the as-grown Fe<sub>4</sub>Se<sub>5</sub> sample.



**Supplementary Figure 5.** The Hall measurement of  $R_{xy}$  v.s. applied magnetic field of (A) the as-grown  $\text{Fe}_4\text{Se}_5$  nanosheet and (B)  $\text{Fe}_4\text{Se}_5$  treated with RTA 450 °C under different temperature